

An induced pluripotent stem cell model of hypoplastic left heart syndrome (HLHS) reveals multiple expression and functional differences in HLHS derived cardiac myocytes

Yan Jiang ^{1,2#}, Saba Habibollah ^{1#}, Katarzyna Tilgner ¹, Joseph Collin ¹, Tomas Barta ¹, Jumana Yousuf Al-Aama ³, Lenka Tesarov ^{1,4}, Rafiqul Hussain ¹, Andrew W. Trafford ⁵, Graham Kirkwood ⁵, Evelyne Sernagor ⁶, Cyril G. Eleftheriou ⁶, Stefan Przyborski ⁷, Miodrag Stojkovic ⁸, Majlinda Lako ¹, Bernard Keavney ^{1,5} and Lyle Armstrong ^{1*}

Authors contributed equally to this work

**To whom correspondence should be addressed*

1. Institute of Genetic Medicine, Newcastle University, Newcastle, United Kingdom
2. Soochow University, 199 Ren Ai Rd, Su Zhou, China
3. Princess Al Jawhara Center of Excellence in Research, King Abdulaziz University, Saudi Arabia
4. Centre for Biomedical Image Analysis, Faculty of Informatics, Masaryk University, Brno, Czech Republic
5. Institute of Cardiovascular Science, Manchester Academic Health Science Centre, CoreTechnology Facility, Manchester, United Kingdom
6. Institute of Neuroscience, Newcastle University, Newcastle, United Kingdom
7. School of Biomedical Sciences, University of Durham, Durham, United Kingdom
8. Department of Human Genetics, University of Kragujevac, Serbia

**** To whom the correspondence should be addressed:***

Dr. Lyle Armstrong
Newcastle University
Institute of Genetic Medicine
International Centre for Life
Central Parkway
Newcastle NE1 3BZ
United Kingdom
Phone: +44-191-241-8695
Fax: +44-191-241-8666
e-mail: Lyle.Armstrong@ncl.ac.uk

Keywords: Hypoplastic left heart syndrome (HLHS), induced pluripotent stem cells (iPSC), cardiac myocytes (CM), cardiac development, pluripotent stem cell differentiation

Abstract

Hypoplastic left heart syndrome (HLHS) is a serious congenital cardiovascular malformation resulting in hypoplasia or atresia of the left ventricle, ascending aorta, aortic and mitral valves. Diminished flow through the left side of the heart is clearly a key contributor to the condition, but any myocardial susceptibility component is as yet undefined. Using recent advances in the field of induced pluripotent stem cells (iPSC), we have been able to generate an iPSC model of HLHS malformation and characterise the properties of cardiac myocytes (CM) differentiated from these and control-iPSC lines. Differentiation of HLHS-iPSC to cardiac lineages revealed changes in the expression of key cardiac markers and a lower ability to give rise to beating clusters when compared to control-iPSC and human embryonic stem cells (hESC). HLHS-iPSC derived CM show a lower level of myofibrillar organisation, persistence of an fetal gene expression pattern, changes in commitment to ventricular versus atrial lineages and display different calcium transient patterns and electrophysiological responses to caffeine and beta-adrenergic antagonists when compared to hESC- and control-iPSC derived CM, suggesting that alternative mechanisms to release calcium from intracellular stores such as the inositol triphosphate receptor may exist in HLHS in addition to the ryanodine receptor thought to function in control-iPSC derived CM. Together our findings demonstrate that CM derived from an HLHS patient demonstrate a number of marker expression and functional differences to hESC/control iPSC derived CM, thus providing some evidence that cardiomyocyte-specific factors may influence the risk of HLHS.

Introduction

Hypoplastic left heart syndrome (HLHS) is characterised by underdevelopment of the left-sided cardiac structures, variably including hypoplasia or atresia of the left ventricle, ascending aorta, and aortic and mitral valves. HLHS is the commonest cause of heart transplantation in infancy and is the cardiovascular malformation most frequently resulting in childhood death (without surgical intervention, HLHS is invariably fatal). There is a substantial familial predisposition to HLHS¹⁻³, though it is not usually a Mendelian condition and first degree relatives of probands with HLHS have a high incidence (11%, versus 1-2% in the general population) of bicuspid aortic valve. Despite this, only a minority of neonates with severe obstruction of left ventricular outflow have HLHS. Diminished flow through the left side of the heart^{1,2} and disruption of genetic networks specific to left ventricular chamber development⁴⁻⁷ have been suggested to cause HLHS. In particular it has been hypothesised that disruption of genetic networks specific to the left ventricular chamber, which depend on the differential expression of such genes as *Tbx5* and *Lrx1*, is also contributory to the pathogenesis of the condition and loss-of-function mutations in the gene *HAND1*, which is expressed in left-sided cardiac structures including the LV myocardium, are present in a proportion of patients with HLHS. One report has noted that HLHS patient cardiac myocytes show inappropriate expression of PECAM-1 (CD31) and indications that the HLHS left ventricle has a gene expression pattern reminiscent of a heart failure or fetal gene expression pattern⁸. As yet however, there is relatively little evidence in favour of the role of CM-specific factors in HLHS risk. We have derived iPSC lines from one HLHS patient who demonstrated mild facial dysmorphism, bilateral hip dislocation, hypoplastic fingernails, mild microcephaly, aortic atresia and mitral atresia who subsequently died at 10 days of age. CM differentiated from these lines show substantial differences to those obtained from hESC⁹

and control-iPSC lines derived from unaffected neonatal human dermal fibroblast (NHDF), supporting the hypothesis that patient specific myocardial developmental factors make a substantial contribution to the development of HLHS.

Materials and methods

Cell source: Dermal fibroblasts derived from the skin biopsy of one HLHS patient (GM12601) were obtained from the Coriell Institute for Medical Research. The patient was clinically diagnosed with hypoplastic left heart syndrome characterised by aortic and mitral atresia. Associated malformations included mild facial dysmorphism, bilateral hip dislocation, hypoplastic fingernails, and mild microcephaly. The patient died ten days after birth.

Derivation, culture and characterisation of human iPSC lines was performed using a polycistronic lentiviral system (Allele Biotech)¹⁰. For more details refer to the **Supplementary Annex**.

Cardiac differentiation of human ESC/iPSC lines and characterisation of cardiac progenitors was carried out as described in¹¹ with full details presented in the **Supplementary Annex**.

DNA fingerprinting and karyotype analysis were performed as described in¹² (for more details refer to **Supplementary Annex**).

Flow cytometric analysis. Human iPSC were cultured under feeder free conditions (matrigel and murine embryonic feeder cells conditioned media) for two passages. Single cell

dissociation was achieved by adding accutase for five minutes and incubating at room temperature. 200,000-500,000 single cells were resuspended in PBS supplemented with 5% FCS and added to a well of a 96-well plate (U shaped). The plate was spun at 200g for five minutes at 4°C and the supernatant was discarded by flicking the whole plate with adherent cells remaining attached to the bottom. Isotype control or conjugated TRA-1-60 (Millipore) and NANOG (Cell Signaling Technologies) were added at dilution of 1:50 followed by incubation on ice for one hour. Cells were rinsed three times with PBS as before and finally resuspended in 0.5 ml of PBS + 5% FCS for FACS analysis using an LSRII analyser (BD Biosciences). At least 10,000 cells were analysed for each experiment. A similar procedure was followed for the NANOG staining with the exception of one additional step of cell permeabilisation and fixation with 2% PFA at 37°C for 10 minutes prior to antibody addition.

Transmission electron microscopy, Measurement of Cytosolic $[Ca^{2+}]$ and Multi-electrode array recordings were used to further characterise hESC/iPSC derived CM (for full details, refer to **Supplementary Annex**).

DNA sequencing of cardiac specific genes. Coding regions of *NKX2.5*, *HAND1* and *HAND2* genes, including exon-intron boundaries were amplified by polymerase chain reaction (PCR) from genomic DNA of control and HLHS patient derived fibroblasts and iPSC and sequenced (for full details, refer to **Supplementary Annex**).

Results and Discussion

Two iPSC clones were derived from one HLHS patient and one unaffected control. Both HLHS clones behaved very similarly so the data are presented as the average of the two clones wherever possible. iPSC derivation efficiency was lower for HLHS (0.0002%) than control-iPSC (0.3%). A recent paper that was published while this manuscript was under review has shown the prevalence of a senescent phenotype in HLHS derived CM and endothelial cells¹³. If this was to be true for fibroblasts derived from HLHS patients, it could explain the low efficiency of iPSC derivation as suggested by Marion *et al.*¹⁴,

All resulting iPSC were highly similar to hESC (H9) (**Figure 1A**). Exogenous transgenes were silenced in all pluripotent iPSC lines (**Figure 1B**). All HLHS iPSC lines were karyotypically normal (**Figure 1C**) and isogenic with the parent fibroblasts (**Suppl. Figure 1**). Flow cytometric analysis for NANOG and TRA-1-60 expression (**Figure 1D**) was performed in all iPSC and only the iPSC lines that showed expression of those markers in more than 90% of the cells were taken forward for further analysis. Pluripotency was further confirmed by multilineage differentiation as embryoid bodies (EBs) followed by expansion in monolayer culture. Immunohistochemical staining for β -III-tubulin, α -fetoprotein and CD31 indicated the presence of differentiated cell types derived from ectoderm, endoderm and mesoderm in all samples (**Figure 2A**). Sub-cutaneous injection of HLHS- and control-iPSC into immunocompromised NOD/SCID mice gave rise to teratomas containing tissues derived from all three embryonic germ layers (**Figure 2B**). These results demonstrated that fully reprogrammed iPSC can be derived from HLHS patients.

We differentiated hESC, HLHS- and control-iPSC lines into CM using protocols published by Keller's group¹¹. We were particularly interested in investigating the differences between HLHS and patient CM as they emerged during human embryonic development and for this reason we focused our studies on the first 21 days of iPSC and ESC

differentiation which has been reported by a large number of studies to be sufficient for cardiac commitment and generation of contracting CM. Contracting clusters containing cells expressing cardiac markers such as α -actinin, cardiac troponin (cTnT) and the early cardiac development transcription factor HAND1¹⁵, could be readily detected by immunohistochemistry from day 10 of differentiation (**Figure 3A**). Quantitative RT-PCR analysis during differentiation suggested that HLHS-iPSC, control-iPSC and hESC down-regulated pluripotency markers as shown by *SOX2* (**Figure 3B**) and *NANOG* expression (**Suppl. Figure 2A**) and formed mesoderm indicated by expression of *BRACHYURY* (**Figure 3B**). We noticed a lower expression of a key marker of cardiac mesoderm, *MESP1* at differentiation day 10 (**Figure 3B**) in addition to delayed and persistent expression of the cardiac progenitor marker, *GATA4* and reduced expression of a more mature CM marker, cardiac troponin (*cTnT*) at days 14 and 21 of differentiation for the HLHS sample. Although ANOVA two factor analysis indicated no significant differences between H9, NHDF and HLHS samples during the differentiation time course for the expression of above mentioned cardiac markers, t- test analysis performed at specific and key time points indicated that the changes observed between HLHS and each of the two controls (NHDF and H9) were significant ($p < .05$). Quantitative RT-PCR analysis also indicates higher than expected expression of PECAM-1 (CD31) and the embryonic atrial myosin essential light chain (*ALC-1*) in HLHS-derived CM compared to hESC and control iPSC lines (**Suppl. Figure 3**) which supports the observations made by Bohlmeier et al⁸ about persistence of fetal gene expression in of the heart of HLHS patients. It is interesting to note higher expression of *MYH6* (fast isoform of the cardiac myosin heavy chain preferentially expressed in developing atria, **Figure 3B**) and decreased expression of *MYH7* (myosin heavy chain beta predominantly expressed in ventricles; **Suppl. Figure 2B**). This was corroborated by flow cytometric analysis of beating clusters, which show reduced cTnT expression and CX43

(found mainly in ventricular myocardium) in parallel to increased expression of CX40 (enriched in atrial CM) and *ANP* (atrial natriuretic peptide; **Figure 3C**).

A number of publications to date have suggested variations between iPSC clones derived from the same patients as well as iPSC lines derived from different patients in the ability to give rise to cardiomyocytes, thus necessitating inclusion of iPSC lines from multiple HLHS patients. This is difficult for congenital diseases such as HLHS where improvement in fetal imaging have actually led to decreased numbers of babies with HLHS. During this study, we have not observed significant differences between iPSC clones derived either from the unaffected control or the HLHS patients. Furthermore, we have not observed significant differences between the H9 human ESC lines and the unaffected control, which lead us to speculate that differences observed between control and HLHS patient are due to the HLHS phenotype rather than intra and inter line variability. It is also encouraging to notice, that another group reported similar differences in gene expression profile and ventricular/atrial commitment of cardiomyocytes using independently derived iPSC clones from two other HLHS patients (Bossman et al. ISSCR poster T-3147, Boston 2013). Together these findings suggest that HLHS may be characterized by impaired differentiation of cardiac lineages affecting multiple steps such as cardiac mesoderm formation, maturation of cardiac progenitors to fully mature CM and commitment to atrial or ventricular phenotype.

Greatly reduced expression of CX43 has been observed in HLHS cardiac myocytes by other workers.¹⁶ CX43 functions in the electromechanical transduction and signaling between cardiomyocytes to facilitate maturation, alignment, and proliferation during development of the myocardium. The reduced CX43 expression shown by HLHS iPSC derived CM supports the possibility that myocardial development may be compromised by failure to correctly align cardiac myocytes. Alternatively, the higher expression of CX40 may indicate that greater numbers of ventricular conduction system (VCS) cardiomyocytes arise during differentiation

of HLHS iPSC. CX40 is a known marker of this latter cell type¹⁷⁻¹⁹ and our observed data support the possibility of increased numbers of VCS cardiomyocytes. Sequencing of coding regions of *NKX2.5*, *HAND1* and *HAND2* revealed no mutations in HLHS patient sample, excluding those genes as causal factors (data not shown).

Transmission electron microscopy (TEM) of hESC and iPSC derived CM revealed that most CM are mononucleated; however, while densely packed parallel myofibrils organized into apparently mature sarcomeres with Z-band formation were observed for hESC- and control-iPSC derived CM (**Figure 4A: a and e**), a more random arrangement of myofibrils was observed in HLHS-iPSC derived CM despite the presence of abundant Z-bands (**Figure 4A: i**). Moreover CM from hESC and control-iPSC show conspicuous rough endoplasmic reticulum and sarcoplasmic reticulum (**Figure 4A: b, c, f, g** indicated by arrows), but these structures are less apparent in HLHS-iPSC derived CM (**Figure 4A: j, k**).

Numbers and beating rates of contractile areas from HLHS-iPSC EBs are substantially lower than those from hESC or control-iPSC (**Figures 4B and C**) prompting detailed examination of CM calcium release characteristics. Spontaneous rhythmic calcium transients were detected in H9, unaffected control and HLHS-iPSC derived CM (**Suppl. Figure 4A**). Interestingly, HLHS-iPSC derived CM show an accelerated rate of Ca^{2+} transient decay compared to control-iPSC derived CM (**Suppl. Figure 4B**). In fully differentiated cardiac muscle, the sarcoplasmic reticulum is the major source of Ca^{2+} required for contraction^{20,21}. HLHS-iPSC derived CM generate calcium transients in the presence of caffeine whereas control-iPSC derived CM do not (**Suppl. Figure 4C**) implying ryanodine receptor dysfunction in HLHS-iPSC derived CM. The contractile areas are still able to beat so an alternative source of calcium such as the inositol triphosphate system may be operative. This is indicated by upregulation of *IP3R* expression in HLHS derived CM compared to control CM (**Suppl. Figure 5**). Multi-electrode array studies of contracting areas also support

sarcoplasmic reticulum dysfunction. Treatment of CM with the β_1/β_2 adrenergic receptor agonist isoproterenol normally increases the contraction frequency by enhancing Ca^{2+} ATPase activity in the sarcoplasmic reticulum²²; however, the beat frequency of HLHS-iPSC derived CM increases only by 9% after isoproterenol treatment compared to 66% for hESC derived CM (**Suppl. Figure 6**). Therefore, it is possible that for HLHS, inositol triphosphate plays an important role in generating calcium transients. This is also an indicator of immature cardiac differentiation. Set against these data is the observation that control-iPSC derived CM only demonstrate 20% increase in beat frequency; however the inability of HLHS-iPSC derived CM to increase their beat frequency is significant.

Summary: We have presented data describing the derivation of two iPSC lines from an HLHS patient and demonstrated that CM derived from these lines show developmental and/or functional defects that could compromise their ability to contribute to cardiogenesis *in vivo*. Our observations of such intrinsic cellular defects correlate with the findings of other groups such as the possibility that gene expression programs more typical of a fetal cardiac phenotype may persist in HLHS-iPSC-derived CM. Further studies are needed to determine if these defects are causative of HLHS not least of which will be the need to derive more patient specific iPSC to address questions of patient genetic background outside the factors responsible for the HLHS phenotype. Differentiation of HLHS-iPSC to CM is a valuable tool in this investigation since it permits examination not only the more mature stages of CM development but also allows us to access several of the cardiac mesoderm cell types that precede CM formation which is not possible from the HLHS patient tissues alone. Comparison of the transcriptomic and functional parameters of such cells will be a useful mechanism through which we may identify candidate genes whose mutations may contribute to the HLHS phenotype.

ACKNOWLEDGMENTS: The authors would like to thank Mr Ian Dimmick and Dr. Owen Hughes for their help with the flow cytometric analysis, Dr, Mauro Santibanez-Coref for help with the statistical analysis, Complement Genomics Ltd for carrying out the DNA fingerprinting analysis, Addgene for provision of the Cre construct, Dr. Kathryn White for help with the TEM and Coriell Cell Repositories for providing the patient fibroblasts. This study was supported by the Newcastle Health Charity funds and the British Heart Foundation (AWT). BK holds a British Heart Foundation Personal Chair.

Conflict of interest: The authors declare no conflict of interest.

References

1. Harh JY, Paul MH, Gallen WJ, Friedberg DZ, Kaplan S. Experimental production of hypoplastic left heart syndrome in the chick embryo. *Am J Cardiol.* 1973;31:51-56
2. deAlmeida A, McQuinn T, Sedmera D. Increased ventricular preload is compensated by myocyte proliferation in normal and hypoplastic fetal chick left ventricle. *Circulation research.* 2007;100:1363-1370
3. D'Alto M, Russo MG, Pacileo G, Paladini D, Romeo E, Sarubbi B, Cardaropoli D, Ricci C, Calabro R. Left ventricular remodelling in outflow tract obstructive lesions during fetal life. *J Cardiovasc Med (Hagerstown).* 2006;7:726-730
4. Hinton RB, Jr., Martin LJ, Tabangin ME, Mazwi ML, Cripe LH, Benson DW. Hypoplastic left heart syndrome is heritable. *Journal of the American College of Cardiology.* 2007;50:1590-1595
5. Hinton RB, Martin LJ, Rame-Gowda S, Tabangin ME, Cripe LH, Benson DW. Hypoplastic left heart syndrome links to chromosomes 10q and 6q and is genetically related to bicuspid aortic valve. *Journal of the American College of Cardiology.* 2009;53:1065-1071
6. Reamon-Buettner SM, Ciribilli Y, Inga A, Borlak J. A loss-of-function mutation in the binding domain of hand1 predicts hypoplasia of the human hearts. *Human molecular genetics.* 2008;17:1397-1405
7. Iascone M, Ciccone R, Galletti L, Marchetti D, Seddio F, Lincesso AR, Pezzoli L, Vetro A, Barachetti D, Boni L, Federici D, Soto AM, Comas JV, Ferrazzi P, Zuffardi O. Identification of de novo mutations and rare variants in hypoplastic left heart syndrome. *Clin Genet.* 2012;81:542-554
8. Bohlmeier TJ, Helmke S, Ge S, Lynch J, Brodsky G, Sederberg JH, Robertson AD, Minobe W, Bristow MR, Perryman MB. Hypoplastic left heart syndrome myocytes

- are differentiated but possess a unique phenotype. *Cardiovasc Pathol*. 2003 Jan Feb;12(1):23-3
- 9 Thomson JA, Itskovitz-Eldor J, Shapiro SS, Waknitz MA, Swiergiel JJ, Marshall VS, Jones JM. Embryonic stem cell lines derived from human blastocysts. *Science (New York, N.Y.)*. 1998;282:1145-1147
 - 10 Jiang Y, Cowley SA, Siler U, Melguizo D, Tilgner K, Browne C, Dewilton A, Przyborski S, Saretzki G, James WS, Seger RA, Reichenbach J, Lako M, Armstrong L. Derivation and functional analysis of patient specific induced pluripotent stem cells as an in vitro model of chronic granulomatous disease. *Stem cells (Dayton, Ohio)*. 2012;30:599-611
 11. Kattman SJ, Witty AD, Gagliardi M, Dubois NC, Niapour M, Hotta A, Ellis J, Keller G. Stage-specific optimization of activin/nodal and bmp signaling promotes cardiac differentiation of mouse and human pluripotent stem cell lines. *Cell stem cell*. 2011;8:228-240
 12. Stojkovic M, Lako M, Stojkovic P, Stewart R, Przyborski S, Armstrong L, Evans J, Herbert M, Hyslop L, Ahmad S, Murdoch A, Strachan T. Derivation of human embryonic stem cells from day-8 blastocysts recovered after three-step in vitro culture. *Stem cells (Dayton, Ohio)*. 2004;22:790-797
 13. Gaber N, Gagliardi M, Patel P, Kinnear C, Zhang C, Chitayat D, Shannon P, Jaeggi E, Tabori U, Keller G, Mital S. Fetal Reprogramming and Senescence in Hypoplastic Left Heart Syndrome and in Human Pluripotent Stem Cells during Cardiac Differentiation. *Am J Pathol*. 2013 Jul 17. pii: S0002-9440(13)00411-2
 14. Marión RM, Strati K, Li H, Murga M, Blanco R, Ortega S, Fernandez-Capetillo O, Serrano M, Blasco MA. A p53-mediated DNA damage response limits

- reprogramming to ensure iPS cell genomic integrity. *Nature*. 2009 Aug 27;460(7259):1149-53
15. Vincentz JW, Barnes RM, Firulli AB. Hand factors as regulators of cardiac morphogenesis and implications for congenital heart defects. *Birth defects research. Part A, Clinical and molecular teratology*. 2011;91:485-494
 16. Mahtab EA, Gittenberger-de Groot AC, Vicente-Steijn R, Lie-Venema H, Rijlaarsdam ME, Hazekamp MG, Bartelings MM. Disturbed myocardial connexin 43 and N-cadherin expressions in hypoplastic left heart syndrome and borderline left ventricle. *J Thorac Cardiovasc Surg*. 2012 Dec;144(6):1315-227
 17. Miquerol L, Bellon A, Moreno N, Beyer S, Meilhac SM, Buckingham M, Franco D, Kelly RG. Resolving cell lineage contributions to the ventricular conduction system with a Cx40-GFP allele: a dual contribution of the first and second heart fields. *Dev Dyn*. 2013 Jun;242(6):665-778
 18. Harris BS, Spruill L, Edmonson AM, Rackley MS, Benson DW, O'Brien TX, Gourdie RG. Differentiation of cardiac Purkinje fibers requires precise spatiotemporal regulation of Nkx2-5 expression. *Dev Dyn*. 2006 Jan;235(1):38-49.
 19. Desplantez T, McCain ML, Beauchamp P, Rigoli G, Rothen-Rutishauser B, Parker KK, Kleber AG. Connexin43 ablation in foetal atrial myocytes decreases electrical coupling, partner connexins, and sodium current. *Cardiovasc Res*. 2012 Apr 1;94(1):58-65
 20. Trafford AW, Díaz ME, Negretti N, Eisner DA. Enhanced Ca²⁺ current and decreased Ca²⁺ efflux restore sarcoplasmic reticulum Ca²⁺ content after depletion. *Circ Res*. 1997; 81(4):477-84.
 21. Walden AP, Dibb KM, Trafford AW. Differences in intracellular calcium homeostasis between atrial and ventricular myocytes. *J Mol Cell Cardiol*. 2009; 46(4):463-73.

22. Ginsburg KS, Bers DM. Modulation of excitation-contraction coupling by isoproterenol in cardiomyocytes with controlled sr ca^{2+} load and ca^{2+} current trigger. *The Journal of physiology*. 2004;556:463-480.

Figure legends

Figure 1. Molecular characterisation of human iPSC lines derived from HLHS patient and unaffected control. **(A)** Staining of NHDF derived control- and HLHS-iPSC lines and H9 hESC with pluripotency markers and alkaline phosphatase (AP). DAPI staining of nuclei is shown in blue. This is a representative example of at least three independent experiments. Scale bar, 100 μ m; **(B)** quantitative RT-PCR analysis for the expression of total and endogenous *c-MYC* and *SOX2* relative to *GAPDH* with H9 as calibrator (set to 1). Data is presented as mean \pm SEM, n=3; **(C)** A representative example of karyotypic analysis of HLHS-iPSC1 showing a normal 46 XY karyotype; **(D)** Flow cytometric analysis for expression of TRA-1-60. The red line represents the cell population stained with the isotype control and the green line the control sample stained with TRA-1-60 antibody. This is a representative example of at least three independent replicates with the NHDF1 iPSC clone.

Figure 2. **(A) *In vitro* and *in vivo* differentiation capacity of hESC, NHDF derived control- and HLHS-iPSC lines.** *In vitro* differentiation capacity to all three germ layers demonstrated by immunocytochemical staining with an anti-AFP antibody (endoderm), anti-CD31 antibody (mesoderm) and anti- β III-Tubulin antibody TUJ1 (ectoderm). DAPI staining of nuclei is shown in blue. This is a representative example of at least three independent experiments. Scale bar, 100 μ m; **(B) *In vivo* differentiation of hESC line H9 (upper panel), NHDF1-iPSC (middle panel) and HLHS1-iPSC (lower panel).** All three pluripotent stem cell lines produced teratomas containing structures representative of each germ layer, notably neuroepithelium (a,d and g: *ectoderm*), kidney/gut wall (b,e/h respectively; both *endoderm*) and cartilage (c, f and i: *mesoderm*). Histological staining: Masson's Trichrome for iPSC-HLHS mesoderm and Weigert's stain for all other sections. Scale bars: NHDF1-iPSC and iPSC-HLHS 150 μ m, the rest are 75 μ m.

Figure 3. Differentiation of NHDF derived control-iPSC, HLHS-iPSC and H9 hESC to CM *in vitro*. (A) Staining with cardiac markers α -actinin, cTnT and HAND1. Please note a mixed expression pattern of HAND1 in nucleoli and nucleus as previously described in literature. DAPI staining of nuclei is shown in blue. This is a representative example of at least three independent experiments. Scale bar, 100 μ m; (B) Quantitative RT-PCR analysis showing changes in cardiac marker expression during the differentiation of iPSC and hESC lines. Human embryonic heart cDNA was used as calibrator for *MESPI1*, *GATA4*, *cTnT* and *MYH6* whilst hESC cDNA was used as calibrator for *SOX2* and *BRACHYURY*. The calibrator value was set to the value of 1 and all other data was calculated with respect to that. Data are presented as mean \pm SEM, n=6. * indicates significant differences in expression between HLHS and each of the controls: H9 and NHDF as revealed by t-test at the particular time point of differentiation; (C) Flow cytometry data analysis of cardiac markers demonstrating changes in expression profiles of HLHS-iPSC derived CM when compared to control derived cells at day 21 of differentiation. Data are presented as mean \pm SEM, n=6. Anova single factor analysis followed by Bonferroni post hoc test indicated significant differences between HLHS and each of the controls (H9 and NHDF) but no differences between NHDF and H9. For simplicity, only *p< .05 is indicated for the comparison between NHDF and HLHS iPSC lines.

Figure 4. (A) Transmission electron microscopy analysis of CM derived from control- and HLHS-iPSC derived cells and H9 hESC line at day 21 of differentiation. Left column shows highly organized, densely packed, paralleled myofilaments in H9 and NHD1-CM with obvious z-bands (a and e); Less organised sarcomeres (indicated by black arrows, panel i) are observed in the HLHS-derived CM. N= nuclei, ER – endoplasmic reticulum, M – mitochondria, L – lipids, z- z bands. This is a representative example of at least three independent experiments; (B) **Analysis of beating EBs derived from H9, control iPSC (NHDF) and HLHS patient specific iPSC lines.** Schematic presentation of percentage of beating EBs throughout differentiation window (300 EBs were analysed for each time point). Data are presented as mean \pm SEM, n=6. Anova two factor with replication followed by Bonferroni post hoc test indicated significant differences between HLHS and NHDF (p=0.006) and HLHS and H9 (p=0.005); (C) **Analysis of beating rate at day 21 of differentiation time course (100 EBs were analysed in each experiment, n=6).**

Suppl. Figure 1. Representative DNA fingerprinting analysis showing that HLHS-iPSC 1 and 2 are genetically identical to the patient fibroblast.

Suppl. Figure 2. Quantitative RT-PCR analysis for the expression of (A) *NANOG* during iPSC and hESC differentiation timecourse and (B) *MYH7* at day 21 of differentiation. Data are presented as mean \pm SEM, n=6. Calibrator sample for (A) undifferentiated hESC cDNA and for (B) Human embryonic heart cDNA. (B) Anova single factor analysis followed by Bonferroni post hoc test indicated significant differences between HLHS and each of the controls (H9 and NHDF) but no differences between NHDF and H9. For simplicity, only $*p < .05$ is indicated for the comparison between NHDF and HLHS iPSC lines.

Suppl. Figure 3. Quantitative RT-PCR analysis for the expression of *CD31* and *ALC-1* at day 21 of differentiation. Data are presented as mean \pm SEM, n=6. Calibrator sample: human embryonic heart cDNA. T-test was used to analyse the significance between NHDF and HLHS for each of the genes analysed.

Suppl. Figure 4. Characterisation of spontaneous Ca^{2+} oscillations from embryoid body derived CM. (A) Confocal line scan images showing changes in intracellular Ca^{2+} with each contraction; (B) Data showing mean \pm SEM summarising Ca^{2+} transient amplitude (upper panel, pseudo-ratio units), the period of spontaneous Ca^{2+} oscillations (middle panel) and time taken for the Ca^{2+} transient to decay by 90%; (C) Spontaneous Ca^{2+} changes presented as pseudo-ratio (F/F_{rest}) units obtained under baseline conditions (left hand panels), following caffeine mediated inhibition of ryanodine receptor mediated Ca^{2+} release from internal stores (middle panels) and wash-off of caffeine (DMEM, right panels). Note that in the NHDF-control-iPSC EB, caffeine immediately and permanently prevented all spontaneous Ca^{2+} oscillations (upper panels) whereas in the HLHS-iPSC EB (lower panels) rhythmic spontaneous Ca^{2+} oscillations, at a reduced frequency, were still observed in the presence of caffeine suggestive of the presence of alternative Ca^{2+} sources in the HLHS-iPSC derived CM. These are representative examples from at least three independent experiments performed in H9 and NHDF1- and HLHS1-iPSC derived beating EBS.

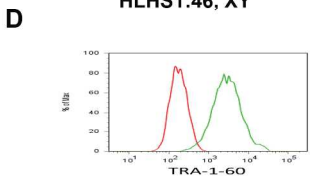
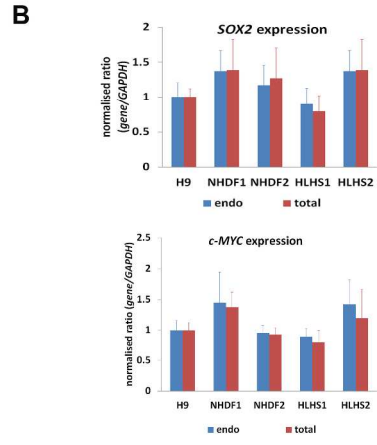
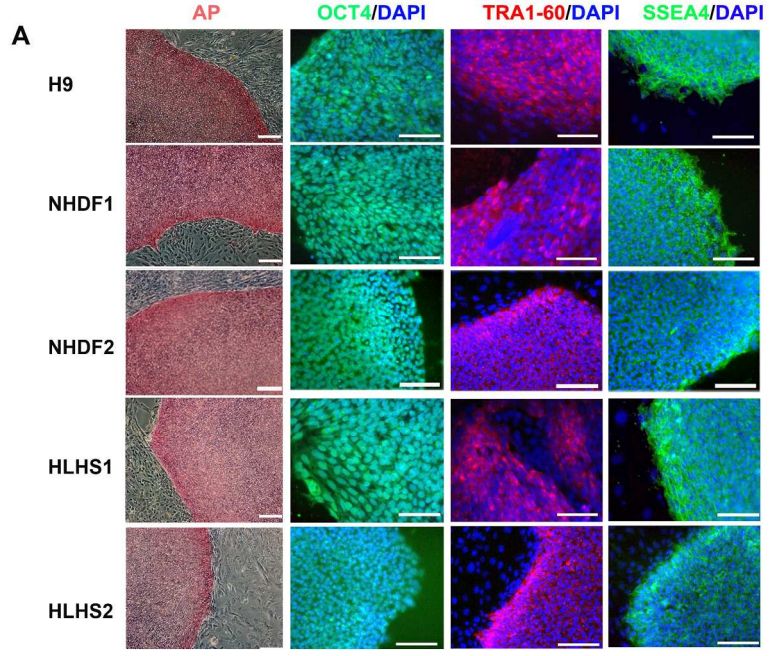
Suppl. Figure 5. Quantitative RT-PCR analysis for the expression of *IP3R* at day 21 of differentiation. Data are presented as mean +/- SEM, n=6. Calibrator sample: hESC cDNA day 21. Anova single factor analysis followed by Bonferroni post hoc test indicated significant differences between HLHS and each of the controls (H9 and NHDF) but no differences between NHDF and H9.

Suppl. Figure 6. Field potential recordings from H9, NHDF control-iPSC and HLHS-iPSC spontaneously beating EBs at day 21 of differentiation and their responses to an adrenergic agonist (isoproterenol). Panels A and B respectively represent responses before and after isoproterenol administration. Recordings were performed for three biological replicates. These are representative examples from at least three independent experiments performed in H9 and NHDF1- and HLHS1-iPSC derived beating EBS.

Suppl. Table 1. Summary of all the oligonucleotides used for RT-PCR.

Suppl. Table 2. Summary of all the oligonucleotides used for mutation screening analysis.

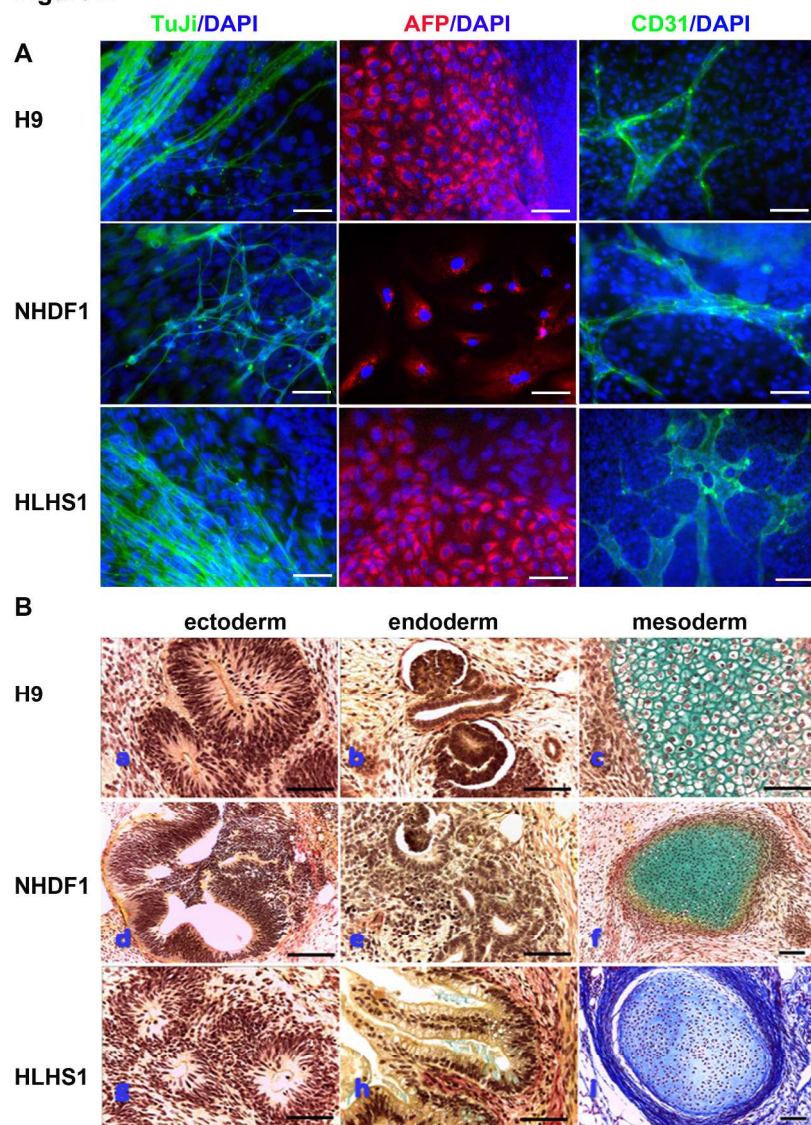
Figure 1



Jiang et al. 2013

209x297mm (300 x 300 DPI)

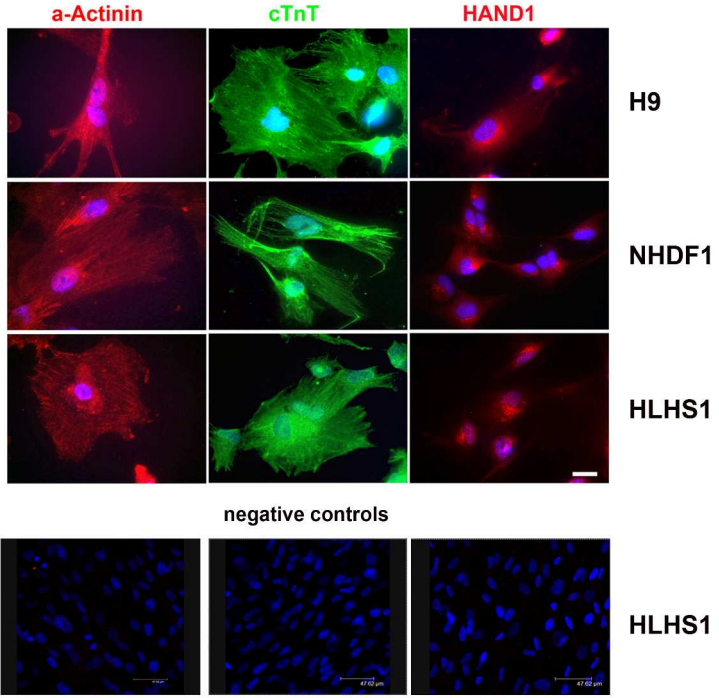
Figure 2



Jiang et al. 2013

209x297mm (300 x 300 DPI)

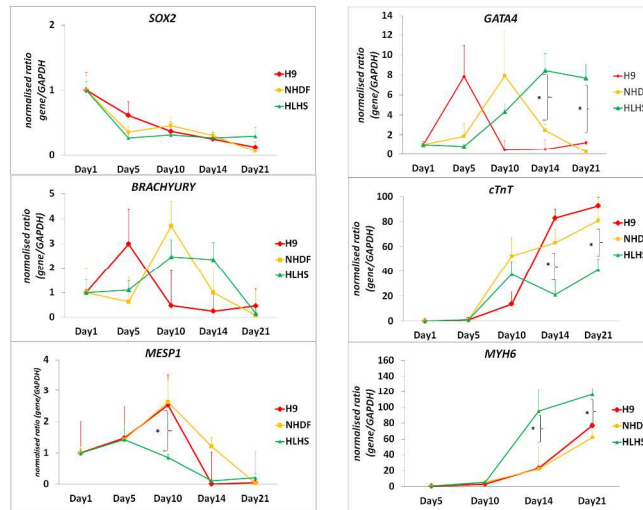
Figure 3A



Jiang et al. 2013

209x297mm (300 x 300 DPI)

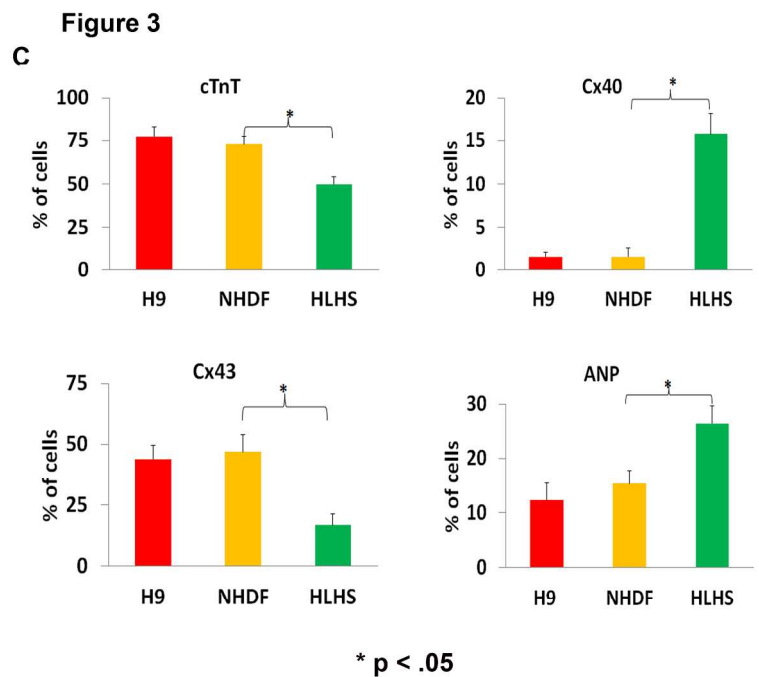
Figure 3B



* p < .05

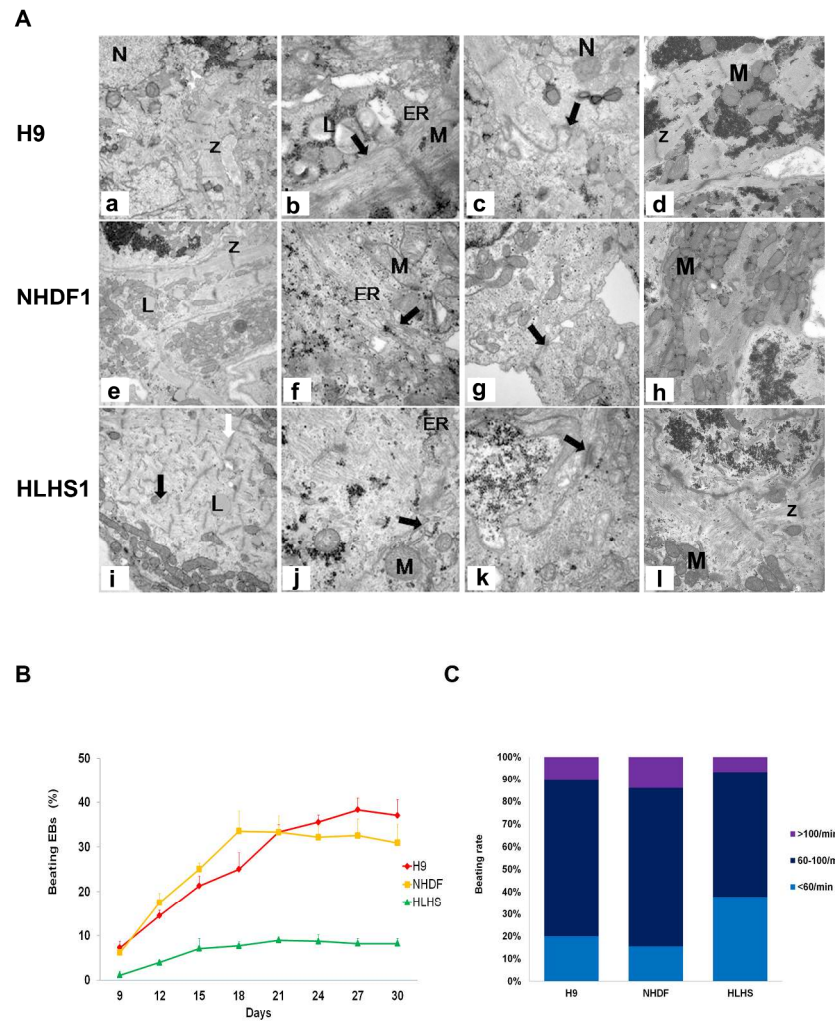
Jiang et al. 2013

209x297mm (300 x 300 DPI)



Jiang et al. 2013

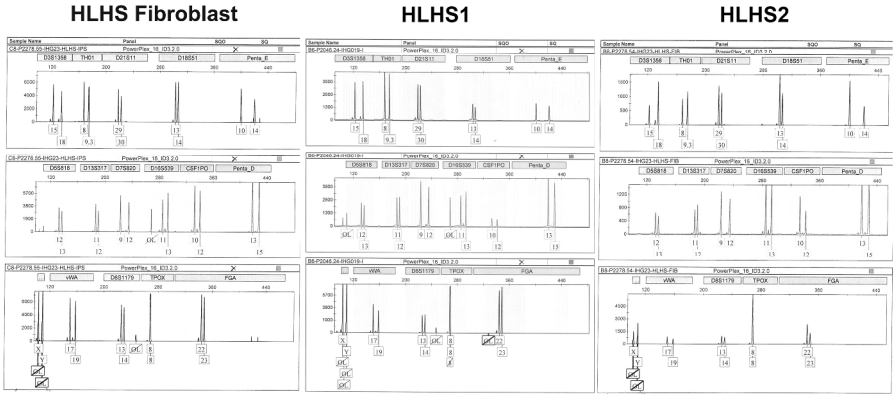
Figure 4



Jiang et al. 2013

209x297mm (300 x 300 DPI)

Supplementary Figure 1

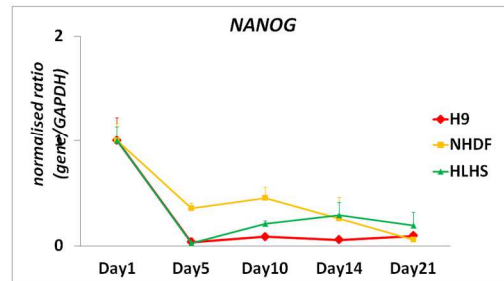


Jiang et al. 2013

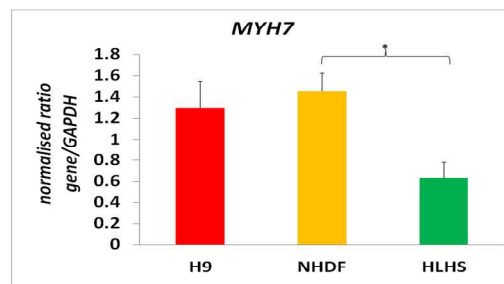
297x209mm (300 x 300 DPI)

Suppl. Figure 2

A



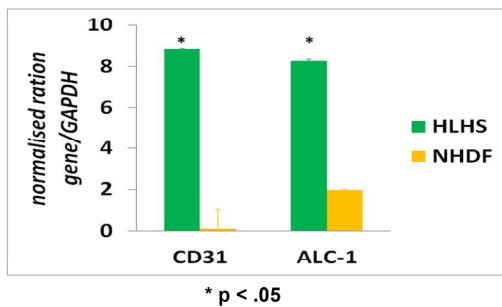
B

* $p < .05$

Jiang et al. 2013

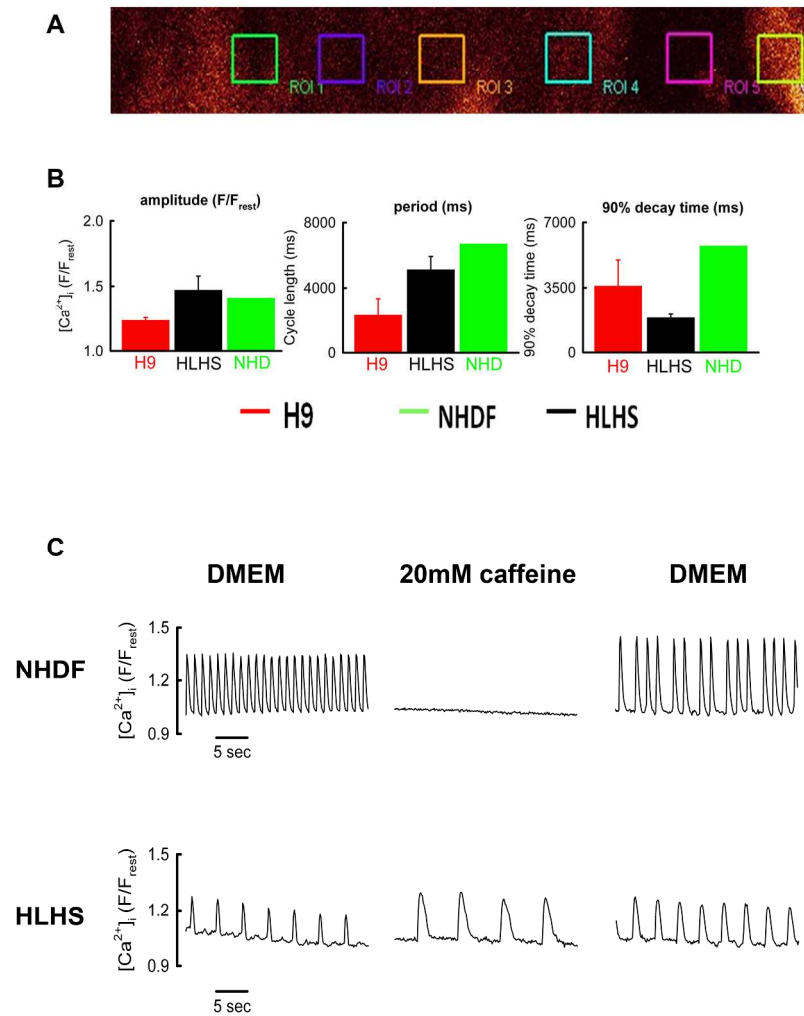
209x297mm (300 x 300 DPI)

Suppl. Figure 3



Jiang et al. 2013

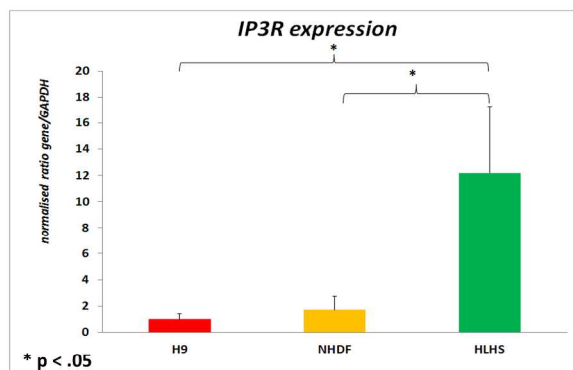
Suppl. Figure 4



Jiang et al. 2013

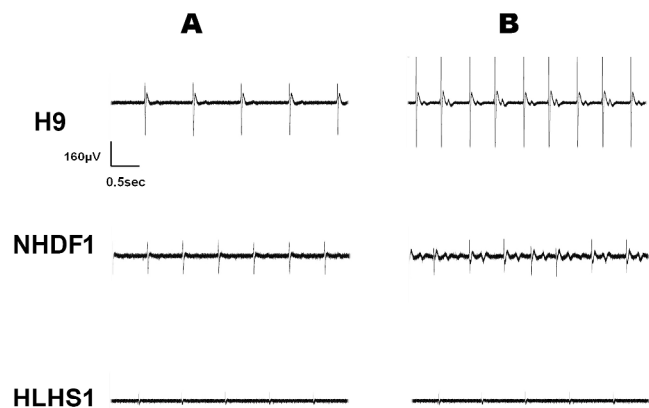
209x297mm (300 x 300 DPI)

Suppl. Figure 5



Jiang et al. 2013

Suppl. Figure 6



Jiang et al. 2013

<i>IP3R</i> Forward	GAAGAACTACAGCACGCTG
<i>IP3R</i> Reverse	TTCTCCAGTAAAGCAGGTAA
<i>BRACHYURY</i> Forward	TGA GGA GAT TAC AGC CCT TAA A
<i>BRACHYURY</i> Reverse	GGT TCC TTA GAG CTG GGT AC
<i>GATA4</i> Forward	CCC TAC CCA GCC TAC ATG G
<i>GATA4</i> Reverse	ACA TAT CGA GAT TGG GGT GTC T
<i>ISL-1</i> Forward	TTG TAC GGG ATC AAA TGC GCC AAG
<i>ISL-1</i> Reverse	AGG CCA CAC AGC GGA AAC A
<i>cTNT</i> Forward	TTC ACC AAA GAT CTG CTC CTC GCT
<i>cTNT</i> Reverse	TTA TTA CTG GTG TGG AGT GGG TGT GG
<i>MYH6</i> Forward	TCAGCTGGAGGCCAAAGTAAAGGA
<i>MYH6</i> Reverse	TTCTTGAGCTCTGAGCACTCGTCT
<i>MYH7</i> Forward	TCGTGCCTGATGACAAACAGGAGT
<i>MYH7</i> Reverse	ATACTCGGTCTCGGCAGTGACTTT
<i>NANOG</i> Forward	GCG GAC TGT GTT CTC TCA GGC
<i>NANOG</i> Reverse	TTC CAG ATG CGT TCA CCA GAT AG
<i>SOX2</i> endo Forward	GGCGCTTTCAGGAAGTTTG
<i>SOX2</i> endo Reverse	GCAAGAAGCCTCTCCTTGAA
<i>SOX2</i> total Forward	AACCCCAAGATGCACAACCTC
<i>SOX2</i> total Reverse	TCTCCGTCTCCGACAAAAGT
<i>c-MYC</i> endo Forward	GAA CTT ACA ATC TGC GAG CC
<i>c-MYC</i> endo Reverse	AGT CGA GGT CAT AGT TCC TG
<i>c-MYC</i> total Forward	TCAAGAGGCGAACACACAAC
<i>c-MYC</i> total Reverse	GGCCTTTTCATTGTTTTCCA
<i>CD31</i> Forward	TCAAATGATCCTGCGGTATTC
<i>CD31</i> Reverse	CCACCACCTTACTTGACAGGA
<i>ALC-1</i> Forward	GGTAAGAGCGTAGGTGAATCCC
<i>ALC-1</i> Reverse	TTACTGCGGCTTCATACTGAGG
<i>VLC-1</i> Forward	AGATCACCTACGGGCAGTGT
<i>VLC-1</i> Reverse	AGTCCATCATCTTGGTATTGAGC

Supplementary Table 1. Summary of oligonucleotides used in the qRT-PCR analysis.

Suppl. Table 2. The sequence of oligonucleotides used for the mutation screening analysis.

Gene	Exon	Primers (5'→3')	Length (bp)	Annealing temp(°C)
<i>HAND1</i>	799	5'-TGA GCG TAA AAC CTG GGA TAG -3' 5'- GAA GTA GGG CCT TTC CTG ATG -3'	470	53.2
<i>HAND1</i>	799	5'- GCA TGG AGC GGC GTT AAT AG -3' 5'- GCG CAG AGT CTT GAT CTT GG -3'	463	58.4
<i>HAND1</i>	799	5'- GGC CCT ACT TCC AGA GCT G -3' 5'- CTA CCT GCA TGG CCT GAG -3'	499	58.4
<i>HAND1</i>	938	5'- TCA TCT TAC CCC ATG CCG G -3' 5'- GTG CGT CTT TGA GCC CTT G -3'	505	61.8
<i>HAND1</i>	938	5'- CAC ACT TGG ATC GCA CGT G -3' 5'- GG CAG CCT TTC ATC TTC CTG -3'	341	61.8
<i>HAND1</i>	938	5'- TTG TCC CTC CAT ATG ATC CG -3' 5'- GAA CAG AGG CTT TCC ACC TAG -3'	526	53.2
<i>HAND2</i>	61	5'-GTT TAT AGC ATG GGG AGG AG -3' 5'- AGA AGT GCC TTA AGG CCC AG -3'	321	51.7
<i>HAND2</i>	107	5'-TCC TGG AAC CCA TCC TCA G -3' 5'- GCA AGT GTC TGT AAA CAC AG -3'	322	53.2
<i>HAND2</i>	1288	5'- GGT AGC GCT AAC CTT GGT AG -3' 5'- AC GGG ATC CCT TAC CAC AC -3'	542	53.2
<i>HAND2</i>	1288	5'- CTG AGG ACT CCT TGC ATT TG -3' 5'-ACT CTT TTG AGG TAT CAG CC -3'	609	53.2
<i>HAND2</i>	1288	5'-GAT GTT TCC AAC AGC CAC TTG -3' 5'- GCC TCA AGA AAT GGC TTC TG -3'	519	58.4
<i>HAND2</i>	1288	5'- GAA CGC TGA GTA GTC TCT AG -3' 5'- CTC TTT AAA TCC GTG GTC TTG -3'	417	58.4
<i>HAND2</i>	2150	5'-TCC AAT TGG GCT GAG AAA TG -3' 5'- AAC TCA GGG CTC AGT CTC TG -3'	421	55.5
<i>HAND2</i>	2150	5'TAA GTC TCG AAG AAG CCC TTG- -3' 5'-AGC TCT ATC CTG CAC CAC TG -3'	392	61.8
<i>NKX2.5</i>	563	5'- CTT CCA AAT GCG TCG TGG C -3' 5'- TGC TGC TGT TCC AGG TTT AG -3'	422	53.2
<i>NKX2.5</i>	563	5'- CAC GCC CTT CTC AGT CAA AG -3' 5'- CAC CAG GCA TCT TAC ATT CTG -3'	449	61.8
<i>NKX2.5</i>	1397	5'-AGC CTG AAA TT TTAAGTCACCG -3' 5'- ACTT GT AGC GCC GGT TCT G -3'	510	58.4
<i>NKX2.5</i>	1397	5'-CAG GTC TAT GAG CTG GAG C -3' 5'-TCG GAT ACC ATG CAG CGT G -3'	522	55.5
<i>NKX2.5</i>	1397	5'- CTA CGG TTA TAA CGC CTA CC -3' 5'- AAA CTC TCC CGT GCG CAA G -3'	412	58.4
<i>NKX2.5</i>	1397	5'-ATT CCG CAG AGC AAC TCG G -3' 5'-TGC CTG AGA TCT GAG ACC AG -3'	599	58.4

Cell culture and lentiviral transductions

Dermal fibroblasts derived from the skin biopsy of one HLHS patient obtained from the Coriell Institute for Medical Research (GM12601) were cultured in tissue culture coated flasks (Iwaki T25) in Iscove's Modified Dulbecco's Medium, plus 10% fetal calf serum (PAA, Somerset, UK), 2 mmol L-glutamine, 0.1 mmol nonessential amino acids and 100 units/mL penicillin (all PAA). Induction of pluripotency was performed using a polycistronic lentiviral vector encoding *OCT4*, *SOX2*, *KLF4* and *c-MYC* under the control of an *EF1 α* promoter (Allele biotech, San Diego, USA) as described in our previous publication⁹. Briefly, fibroblasts were infected with lentiviral particles (MOI=2) with addition of 6 μ g/ml polybrene in Iscove's Modified Dulbecco's Medium, plus 10% fetal calf serum (PAA), 2 mmol L-glutamine, 0.1 mmol nonessential amino acids, 100 units/mL penicillin (PAA) for 48 hrs. Six days after transduction, fibroblasts were disaggregated and plated onto feeder layers of mitotically inactivated mouse embryonic fibroblasts in hESC culture medium (KO-DMEM, 20% Knockout™ Serum Replacement, 0.1 mmol nonessential amino acids, 2 mmol L-glutamine, 100 units/mL penicillin and 10ng/mL human recombinant bFGF) at a density of 8,000 cells per one well of a six well plate. The feeder plates with lentiviral vector treated cells were maintained at 37°C / 5% CO₂ in hESC medium for 2-3 weeks or until colonies of cells with morphology similar to hESC appeared. These were mechanically dissected into several pieces and plated onto fresh feeder cells to develop further colonies for characterisation. In this study, we have used the hESC line, H9 and the neonatal human dermal fibroblast (NHDF)-derived-iPSC as our parallel controls.

Teratoma formation

Approximately 5×10^5 NHDF-derived-iPSC, HLHS-patient-specific iPSC and hESC were injected subcutaneously into the right flanks of adult NOD/SCID mice and maintained for 6-12 weeks. All cells were co-transplanted with 50 μ l Matrigel (BD Biosciences) to enhance teratoma formation. After 8 weeks, mice were sacrificed, teratoma tissues were dissected, fixed in Bouins overnight, processed and sectioned according to standard procedures then counterstained with either haematoxylin and eosin or Massons trichrome stain. Sections (5-8 μ m thick) were examined using bright field light microscopy and photographed as appropriate.

Quantitative RT-PCR

Total RNA was isolated using TRIzol Reagent (Invitrogen) at different points during the differentiation process. Genomic DNA was removed by treatment with DNaseI (Ambion) at 37°C for 30 minutes. Total RNA (1 μ g) was used for reverse transcription using the SuperScript III First strand synthesis system (Invitrogen). Details of the panel of differentiation markers, cardiac specific markers and calcium handling protein genes are listed in **Suppl. Table 1**. Quantitative RT-PCR was performed using an ABI 7900 with the iQ SYBR Green Supermix (Promega). Data was analysed using qBase v1.3.5 and the comparative threshold cycle (Ct) method. In all samples the results were normalised to the expression level of the housekeeping gene *GAPDH*, and referenced to hESC and human embryonic heart cDNA (obtained from Carnegie Stage 14) depending on the gene of interest being analysed.

EB formation and cardiac differentiation

Before EB formation, the iPSC and hESC were cultured in matrigel-coated plates for

3 days to deplete the feeder cells (Day -3). On day 0, the colonies were detached and separated mechanically in small clusters (around 500-1000 cells/per clump), then placed on low attachment plates (Costar) in suspension with differentiation medium consisting of StemPro-34 (Invitrogen), supplemented with 10ng/mL penicillin/streptomycin, 2mmol L-Glutamine, 1mmol ascorbic acid, and 0.4mmol monothioglycerol (MTG) (Sigma). BMP4, Activin A, DKK1, VEGF (R&D systems), SB (Tocris) and b-FGF were added at the indicated time points and concentrations for each cell lines individually as described in literature methods¹⁰. After 7 days in suspension culture, the EBs were plated on 0.1% gelatin-coated 12 well culture plates at the density of 20 EBs per well and cultured in cardiac medium (changed every 2-3 days). The number of contracting EBs and contraction rates were measured every second day using a Zeiss microscope with a heated stage (37°C). Beating areas were usually observed 2 or 3 days after re-plating and reached maximal numbers normally by day 20. These areas were cut carefully and used for other characterisation experiments.

Immunocytochemical analysis

Undifferentiated iPSC and hESC were plated on 4 well plates under feeder free conditions as described above, whilst single cardiac myocytes were isolated from beating areas using Accutase (Invitrogen) digestion for 10 minutes at 37°C followed by plating onto 0.1% gelatin coated chambers with cardiac medium for 2 days to allow cell attachment. Cells were fixed in 4% paraformaldehyde for 10 minutes at room temperature followed by treatment with 0.5% Triton X-100 for 10 minutes. Samples were blocked by incubation with 5% BSA for 1 hour at room temperature. Primary antibodies used in this study are anti-OCT-4 (1:100, Millipore, Watford,

UK), anti-SSEA-4 (1:100, BD Pharmingen), anti-TRA-1-60 (1:100; Millipore), anti-CD31 (1:100, PECAM1), anti- β -III-Tubulin (TUJ1) (1:100; Covance, New Jersey USA), anti-AFP (1:100; Sigma), anti-mouse IgG-FITC conjugated (1:800; Sigma), anti-rabbit rhodamine (1:800). The nuclei were counterstained with 10 μ g/mL Hoechst 33342 (Life Technologies). The bright field and fluorescent images were obtained using a Zeiss microscope and the AxioVision software (Carl Zeiss, Jena, Germany).

All antibodies were checked for specificity on heart sections from human embryos obtained from HDBR (www.hdbr.org).

Flow cytometry

The EB (and/or contractile areas) at different time points were collected and digested with Accutase for 5-7 minutes to obtain a single cell suspension. Cells were washed with PBS and fixed using 4% formaldehyde for 10 minutes followed by permeabilization with methanol for 30 minutes. Samples were incubated with the primary antibodies for 1 hour followed by incubation with an appropriate Alexa fluor 488 conjugated secondary antibody for 30 minutes. DNA staining dye (DAPI) was added before analyzing the samples by flow cytometry (FACS Canto (BD Biosciences, CA, USA). At least 10,000 events were collected and the data was analyzed utilizing FlowJo version 6.4 software. All experiments were performed in triplicate.

DNA fingerprinting

To confirm that HLHS-patient-specific (HLHS1, HLHS2) and unaffected iPSC (NHDF1 and 2) lines were genetically identical to the respective patient dermal fibroblasts, DNA fingerprinting was carried out. Total genomic DNA was extracted from all five samples and amplified with 15 microsatellite markers: D3S1358, TH01,

D21S11, D18S51, Penta-E, D5S818, D13S317, D7S820, D16S539, CSF-1PO, Penta-D, vWA, D8S1179, TPOX and FGA and analysed on an ABI 377 sequence detector using Genotype software (Applied Biosystems, Foster City, CA).

Karyotype analysis of HLHS patient specific and unaffected hiPSC

Karyotypes were determined by standard G-banding procedure, as described in Stojkovic *et al*¹¹.

Transmission electron microscopy

Transmission electron microscopy was performed on day 30 contracting EBs fixed with 2% glutaraldehyde in 0.1M cacodylate buffer. Post fixation was performed at room temperature for 1 hour with 1% osmium and 1.5% potassium ferrocyanide. The samples were dehydrated in graded acetone and embedded in epoxy resin at 60°C. Half micron sections were stained with 1% toluidine blue and ultra-thin sections were cut on Leica EM UC7 ultramicrotome and double stained with 1% uranyl acetate and lead citrate. Ultrastructural examination was performed with Philips CM 100 TEM at 100 kV. Digital images were recorded with an AMT40 CCD camera (Deben).

Measurement of Cytosolic [Ca²⁺]

Beating clusters were micro-surgically dissected and plated on the gelatin covered chamber slide (BD) for cytosolic calcium transient analysis. Briefly, the cells were loaded with Fluo3AM (10 µmol) at 37°C for 40 minutes and allowed to de-esterify for at least 30 mins at 37°C. Spontaneous calcium transients were recorded using a Leica TCS SP2 inverted confocal microscope (excitation 488 nm, emission 510-600 nm; using an HCX APO L U-V-I 40.0x0.80 W objective). To assess the role of the

intracellular Ca^{2+} store, the sarcoplasmic reticular (SR) of beating EBs were superfused with caffeine (20 mmol) to discharge the Ca^{2+} store. Ca^{2+} transients amplitude, period and decay kinetics (single exponential function fitted to decay phase of Ca^{2+} transients) were calculated using custom VBA routines.

Multi-electrode array recordings

To characterize the electrophysiological properties of iPSC derived CM, contracting EBs were dissected and plated on gelatin coated multi-electrode arrays (Multichannel Systems, Reutlingen, Germany) consisting of 60 titanium nitride electrodes (30 μm diameter, 200 μm separation) in a 8x8 configuration without corners. Recordings were performed at a sampling rate of 20 kHz. The recorded electrograms were used to determine the local field potential (FP) duration (FPD). This parameter was previously shown to correlate with the action potential duration and to reflect the local QT interval^{12,13}. To assess the responsiveness of cardiac contractility to β -adrenoceptor stimulation, 20 μL of isoproterenol (Sigma) was added directly to the recording chamber (2 mL volume). Extracellular recordings were performed for 200 seconds in control conditions and at 5 minutes after drug application.

DNA sequencing of cardiac specific genes

Coding regions of *NKX2.5*, *HAND1* and *HAND2* genes from HLHS-patient-specific fibroblasts and iPSC, including exon-intron boundaries were amplified by polymerase chain reaction (PCR) of genomic DNA and sequenced. The sequences of oligonucleotides used for this analysis are shown in **Suppl. Table 2**. PCR was undertaken for 5'-UTR and 3'-UTR of exons 799bp and 938bp of *HAND1*, exons 563bp and 1397bp of *NKX2.5*, and exons 61bp, 107bp, 1288bp and 2150bp of *HAND2*. Neonatal human diploid fibroblasts (NHDF) and NHDF-derived-iPSC were

analysed as controls. PCR products were sequenced commercially (GATC Biotech; www.gatc-biotech.com) and analysed manually to identify sequence differences between the HLHS patient DNA and the one obtained from unaffected control (NHDF).